

Barlowite as a canted antiferromagnet: theory and experiment

Harald O. Jeschke,¹ Francesc Salvat-Pujol,¹ Elena Gati,² Nguyen Hieu Hoang,² Bernd Wolf,² Michael Lang,² John A. Schlueter,³ and Roser Valentí¹

¹*Institut für Theoretische Physik, Goethe-Universität Frankfurt, Max-von-Laue-Straße 1, 60438 Frankfurt am Main, Germany*

²*Physikalisches Institut, Goethe-Universität Frankfurt, Max-von-Laue-Straße 1, 60438 Frankfurt am Main, Germany*

³*Division of Materials Research, National Science Foundation, Arlington, Virginia 22230, USA*

We investigate the structural, electronic and magnetic properties of the newly synthesized mineral barlowite $\text{Cu}_4(\text{OH})_6\text{FBr}$ which contains Cu^{2+} ions in a perfect kagome arrangement. In contrast to the spin-liquid candidate herbertsmithite $\text{ZnCu}_3(\text{OH})_6\text{Cl}_2$, kagome layers in barlowite are perfectly aligned due to the different bonding environments adopted by F^- and Br^- compared to Cl^- . We perform density functional theory calculations to obtain the Heisenberg Hamiltonian parameters of $\text{Cu}_4(\text{OH})_6\text{FBr}$ which has a Cu^{2+} site coupling the kagome layers. The 3D network of exchange couplings together with a substantial Dzyaloshinskii-Moriya coupling lead to canted antiferromagnetic ordering of this compound at $T_N = 15$ K as observed by magnetic susceptibility measurements on single crystals.

PACS numbers: 71.15.Mb, 75.10.Jm, 75.30.Cr, 75.30.Et, 71.20.-b

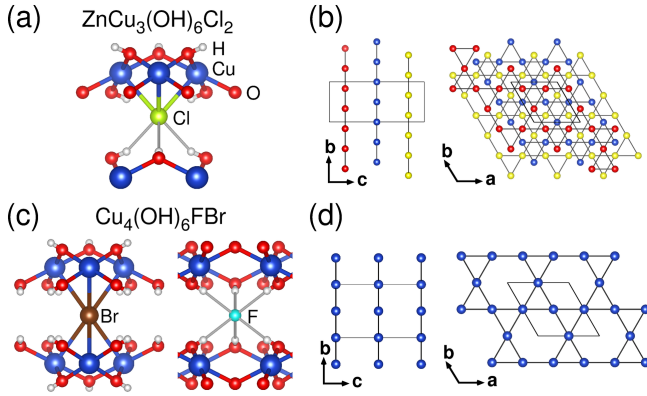


FIG. 1. Chloride environment of herbertsmithite (a) compared to bromide and fluoride environments of barlowite (c). (b) Mix of covalent and hydrogen bonding in $\text{ZnCu}_3(\text{OH})_6\text{Cl}_2$ leads to three kagome layers shifted with respect to each other, as shown by differently colored Cu^{2+} sites. (d) Preference of Br^- for covalent bonding and of F^- for hydrogen bonding leads to perfect alignment of kagome layers in $\text{Cu}_4(\text{OH})_6\text{FBr}$ (only Cu(1) sites are shown here).

Since the successful synthesis of herbertsmithite ($\text{ZnCu}_3(\text{OH})_6\text{Cl}_2$) [1], spin-liquid candidates based on spin-1/2 kagome lattices have been intensively investigated in recent years [2, 3]. The paratacamite family of compounds has proven to be a fertile ground for kagome materials with different properties. The $\text{Zn}_x\text{Cu}_{4-x}(\text{OD})_6\text{Cl}_2$ series of materials has been found to form valence-bond solids due to distortions of the kagome layer in monoclinic space groups [4]. The replacement of Zn^{2+} in $\text{ZnCu}_3(\text{OH})_6\text{Cl}_2$ by a nonmagnetic ion like Mg^{2+} possibly leads to another spin-liquid candidate [5], as does replacement of 2Cl^- by SO_4^{2-} [6]. On the other hand, magnetic ions between the kagome

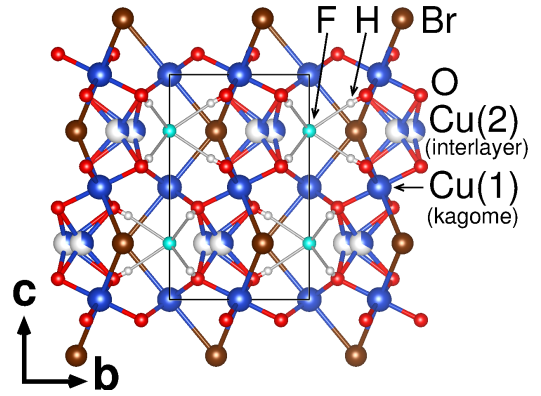


FIG. 2. Crystal structure of $\text{Cu}_4(\text{OH})_6\text{FBr}$ ($P6_3/mmc$ space group, No. 194). Note that the Cu(2) site with Wyckoff position $12j$ is $1/3$ filled.

layers lead to compounds that order magnetically [7]. While realizations of quantum spin liquids have been desperately searched for [8], so far, together with the triangular-lattice molecule-based materials κ -(BEDT-TTF) $_2\text{Cu}_2(\text{CN})_3$ (BEDT-TTF = bis(ethylenedithio)-tetrathiafulvalene) [9], and $\text{EtMe}_3\text{Sb}[\text{Pd}(\text{dmit})_2]_2$ (dmit = 1,3-dithiole-2-thione-4,5-dithiolate, Me = CH_3 , Et = C_2H_5) [10], herbertsmithite has been considered one of the best candidates [11]. However, $\text{ZnCu}_3(\text{OH})_6\text{Cl}_2$ has not been free from controversy as Zn^{2+} and Cu^{2+} are similar in size, and both kagome layers diluted with nonmagnetic Zn^{2+} [3] as well as magnetic Cu^{2+} ions replacing Zn^{2+} between the kagome layers [12] are possible. Therefore, it would be desirable to devise a crystal modification of herbertsmithite that would make the Cu^{2+} and Zn^{2+} sites less similar in order to increase the tendency of Cu^{2+} ions to form the kagome layer as well as the tendency of the nonmagnetic transition metal ion to stay

away from the kagome plane. The purpose of this work is (1) to suggest such a strategy, exemplarily realized in the mineral barlowite and (2) to unveil the microscopic origin of the electronic and magnetic behavior of this system via a combination of density functional theory calculations and magnetic susceptibility measurements. Besides the search for ideal quantum spin liquids, the electronic structure of kagome materials offers a large variety of interesting properties, like for instance the presence of flat bands at certain fillings that induces Nagaoka ferromagnetism [13] or the presence of Dirac points at $4/3$ filling that could lead to unusual symmetry protected metals or superconductors [14].

In herbertsmithite, the Cl^- binding environment is partially covalent, partially hydrogen bonded, as shown in Fig. 1 (a). This leads to a horizontal staggering of kagome layers (Fig. 1 (b)) as Cu^{2+} triangles can be placed either above or below a Cl^- ion, but not both above and below. We suggest using a mixed halide system where the strong hydrogen bond acceptance of the F^- ion is used to create a hydrogen rich pocket with six hydroxyl ions; on the other hand, Br^- can form six covalent bonds to three Cu^{2+} ions above and three below (Fig. 1 (c)). Following this recipe via the chemical synthesis of $\text{Cu}_4(\text{OH})_6\text{FBr}$, we arrive at perfectly aligned kagome planes as shown in Fig. 1 (d). This compound is known as the mineral barlowite [15]. So far, only some of its properties have been reported [16].

Single crystals of barlowite, $\text{Cu}_4(\text{OH})_6\text{FBr}$, were grown synthetically through the hydrothermal reaction of copper carbonate basic (malachite), with perbromic acid in the presence of ammonium fluoride. The crystal structure of $\text{Cu}_4(\text{OH})_6\text{FBr}$ was determined by single crystal X-ray diffraction measurements [17] at ambient temperature and is shown in Fig. 2. Barlowite crystallizes in $P6_3/mmc$ symmetry with each intralayer Cu^{2+} ($\text{Cu}(1)$) ion lying on a site of $2/m$ symmetry (see Table I). This intralayer Cu^{2+} exhibits a strongly tetragonally distorted octahedral coordination with four equatorial Cu-O bonds of $1.954(1)$ Å and two axial Cu-Br bonds of 3.022 Å. Interlayer Cu^{2+} ($\text{Cu}(2)$) sites lie on a general position and are thus $1/3$ occupied and disordered over three equivalent positions.

TABLE I. Structural parameters for $\text{Cu}_4(\text{OH})_6\text{FBr}$ at $T = 298(2)$ K ($P6_3/mmc$ space group, $a = 6.799(4)$ Å, $c = 9.3063(13)$ Å, $Z = 2$). In this table, U is the anisotropic displacement parameter (isotropic for H).

Atom	Site	x	y	z	U (Å ²)	Occ.
Cu(1)	6g	0.5000	0	0	0.01540(17)	1
Cu(2)	12j	0.62884(12)	0.2577(2)	$1/4$	0.0133(4)	$1/3$
O	12k	0.79768(18)	0.20232(18)	0.0916(2)	0.0137(4)	1
H	12k	0.852(3)	0.148(3)	0.127(4)	0.021	1
Br	2c	$1/3$	$2/3$	$1/4$	0.0184(2)	1
F	2b	0	0	$1/4$	0.0238(10)	1

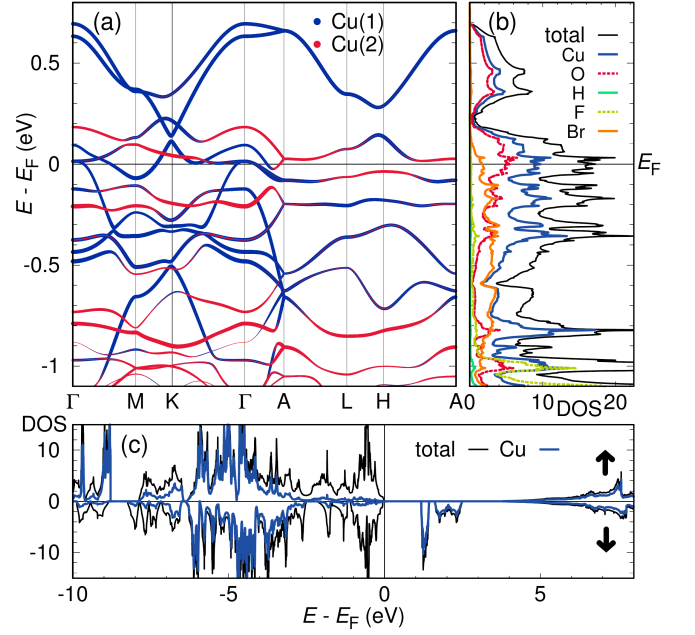


FIG. 3. (a) GGA band structure and (b) GGA density of states (DOS) of $\text{Cu}_4(\text{OH})_6\text{FBr}$. DOS is given in states per eV and formula unit. High symmetry points $M = (1/2, 0, 0)$, $K = (1/3, 1/3, 0)$, $A = (0, 0, 1/2)$, $L = (1/2, 0, 1/2)$, $H = (1/3, 1/3, 1/2)$ were chosen to reflect the $P6_3/mmc$ symmetry of the real material rather than the $Cmcm$ symmetry used for computational purposes. (c) GGA+U density of states for $U = 6$ eV, $J_H = 1$ eV and ferromagnetic order. Note that the size of the gap is related to the value of U considered.

In order to characterize barlowite electronically and magnetically, we combined first principles density functional theory (DFT) calculations with susceptibility measurements. Our DFT calculations were performed on the basis of the full-potential non-orthogonal local-orbital basis (FPLO) [18], employing the generalized gradient approximation (GGA) [19] as well as GGA+U [20] functionals. The Hubbard parameter U was set to 6 eV, the Hund's rule coupling J_H to 1 eV. The exchange-coupling constants between spin-1/2 Cu^{2+} ions were obtained by mapping GGA+U total energy differences of several Cu^{2+} spin configurations onto a spin-1/2 Heisenberg model [21, 22]. In order to make a sufficient number of Cu^{2+} sites inequivalent to allow for various spin configurations, the symmetry was lowered from the $Cmcm$ to the Cm space group (No. 8) containing 6 inequivalent Cu^{2+} positions.

In Fig. 3 (a)-(b) we show first the GGA band structure and density of states of barlowite. The main contribution near the Fermi level is of Cu 3d orbitals hybridized with O 2p orbitals. The band structure along the high-symmetry path Γ -M-K- Γ reflects the dispersion of the kagome layers (dominated by Cu(1) d states) while the band structure along the high-symmetry path A-L-H-A at $k_z = 0.5$ arises from the 2D lattice formed by the inter-kagome

TABLE II. Exchange coupling constants for $\text{Cu}_4(\text{OH})_6\text{FBr}$, calculated with GGA+U at $U = 6$ eV, $J_H = 1$ eV and with atomic-limit double-counting correction.

Name	$d_{\text{Cu-Cu}}$ (Å)	Type	J_i (K)
Kagome layer coupling			
J_3	3.3399	Cu(1)-Cu(1)	177
Interlayer couplings			
J_1	2.7632	Cu(1)-Cu(2)	-205
J_2	3.1885	Cu(1)-Cu(2)	-32
J_4	4.6532	Cu(1)-Cu(1)	5
J_6	5.5264	Cu(2)-Cu(2)	16

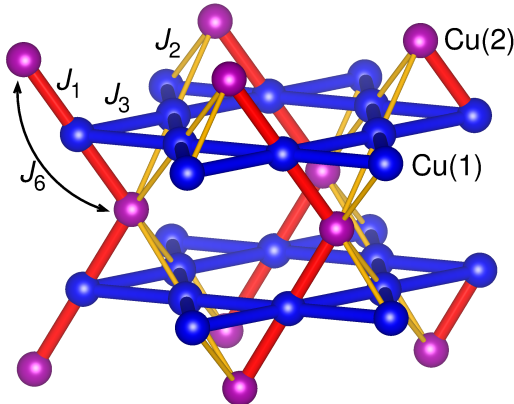


FIG. 4. Important exchange paths of $\text{Cu}_4(\text{OH})_6\text{FBr}$. The notation J_i , $i = 1, 2, 3, \dots$ denotes 1st, 2nd, 3rd, ... Cu-Cu neighbors. Positive (negative) J values denote antiferromagnetic (ferromagnetic) couplings. Exchange constants were determined to be $J_3 = 177$ K (kagome layer), $J_1 = -205$ K and $J_2 = -32$ K. A coupling $J_6 = 16$ K connecting two Cu(2) sites along the red bond is indicated by a curved arrow. Note that disordered Cu(2) sites in the $P6_3/mmc$ space group lead to random permutations of the two weak and one strong ferromagnetic couplings between every Cu(1) triangle above and below a Cu(2) site. Larger couplings are shown with cylinders of larger diameter.

Cu(2) atoms. We observe that the electronic structure of the kagome layer resembles the electronic structure of the spin-liquid compound herbertsmithite very well [22]. However, both herbertsmithite and barlowite are Mott insulators. In order to reflect this behavior in the band structure calculations we show in Fig. 3 (c) the density of states calculated with the GGA+U functional with $U = 6$ eV.

The exchange couplings we obtain from total energy calculations are listed in Table II. The nearest neighbor coupling in the kagome plane is $J_3 = 177$ K for barlowite. This is very similar to the value $J = 182$ K obtained for herbertsmithite, reflecting the fact that Cu-O-Cu angles are very similar in both compounds (117° in barlowite, 119° in herbertsmithite). The fact that barlowite has Cu^{2+} ions at interlayer positions (Cu(2)) determines

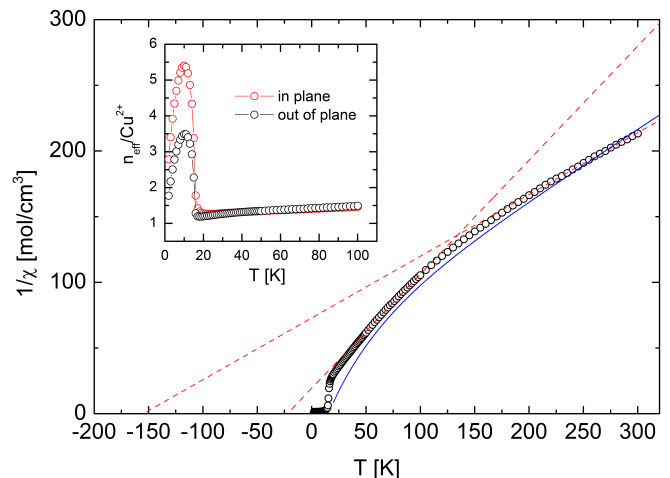


FIG. 5. Inverse molar susceptibility as a function of temperature (open circles) taken at $B = 0.1$ T for $B \parallel c$ together with Curie-Weiss fits (red broken lines) for $200 \text{ K} \leq T \leq 300 \text{ K}$ and $50 \text{ K} \leq T \leq 100 \text{ K}$. Also shown is a theoretical approximation to $1/\chi$ calculated by 10th-order high-temperature series expansion [23], using the calculated value $J_3 = 177$ K and $J_1 = -0.94J_3$, $J_2 = -0.16J_3$ and $J_6 = 0.15J_3$ as well as a g factor of 2.20 (blue solid line). Note that J_1 , J_2 and J_6 agree with the calculated values within their error bars. Inset: Effective magnetic moment per Cu^{2+} ion as a function of temperature in fields $B = 0.1$ T for $B \parallel c$ and $B \perp c$ both after cooling in zero field (ZFC).

the magnetic behavior of this system at low temperatures. Specifically, we find that ferromagnetic interlayer couplings ($J_1 = -205$ K and $J_2 = -32$ K) exist between Cu(1) (in the kagome layer) and Cu(2) (interlayer). Further exchange paths become increasingly and significantly weaker – comparable or smaller than $0.1J$. Within the Cm unit cell chosen here, it was not possible to separate the coupling J_5 corresponding to a Cu(1)-Cu(2) distance of 5.2359 Å from the small ferromagnetic J_2 . The vertical coupling J_4 between the kagome planes is negligibly small. The resulting Heisenberg Hamiltonian parameters are illustrated in Fig. 4. Note that due to the lowering of the symmetry from $P6_3/mmc$ to $Cmcm$ for the calculations, the path of the ferromagnetic one-dimensional Cu(2) chains has become uniquely defined. In reality, these chains wiggle through the crystal according to the actual positions of Cu(2) which is randomly chosen from the three possible sites. We estimate an error bar on the Heisenberg Hamiltonian parameters of the order of 20% and possibly larger for the smaller couplings because the calculated values depend strongly on the essentially unknown size of the Hubbard parameter U and because of the tendency of DFT to overestimate the stability of the ferromagnetic state.

The magnetic properties of barlowite were measured using a commercial Quantum Design SQUID magnetometer in the temperature range $2 \text{ K} \leq T \leq 300 \text{ K}$ on

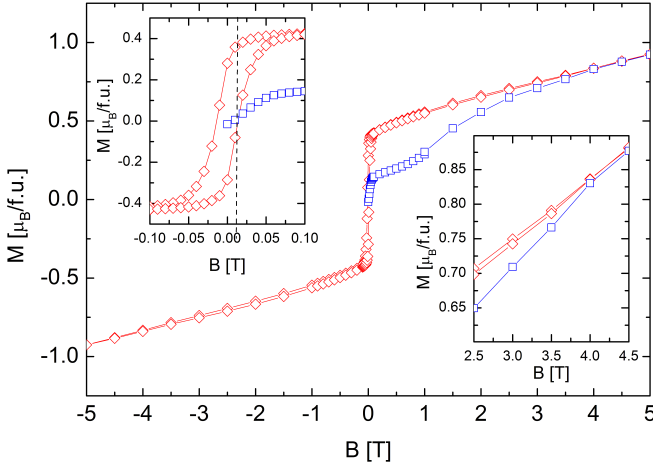


FIG. 6. Magnetization as a function of magnetic field B measured for $B \parallel c$ at $T = 2$ K. The blue open squares correspond to the virgin curve taken after cooling in zero field, the red diamonds correspond to data taken upon subsequent field cycling. Lower right inset: blow-up of high-field section. Upper left inset: blow-up of low-field section.

a single crystal of mass $m = 3.4$ mg. The susceptibility measurements were performed in various fields up to 1 T with B oriented in plane and along the hexagonal c -axis. For the latter orientation the magnetization was measured in fields up to ± 5 T. The experimental data have been corrected for the temperature-independent diamagnetic core contribution of the constituents [26] and the magnetic contribution of the sample holder.

Figure 5 shows the inverse molar magnetic susceptibility (open circles) as a function of temperature for $B \parallel c$. The $1/\chi_{\text{mol}}$ data can be approximated by a Curie-Weiss-like behavior (red broken lines in Fig. 5) at the upper and lower ends with an antiferromagnetic Weiss-temperature $\theta = (155 \pm 2)$ K for $200 \text{ K} \leq T \leq 300 \text{ K}$ and (22 ± 2) K for $50 \text{ K} \leq T \leq 100 \text{ K}$. This behavior is consistent with the presence of two dominant magnetic coupling constants of different sign, suggested by our DFT calculation.

By considering the exchange parameters obtained from DFT, we calculated $1/\chi_{\text{mol}}$ using 10th-order high-temperature series expansion [23]. We find that a very good fit of the experimental observations, shown by the solid blue line in Fig. 5, is obtained with $J_3 = 177$ K and $J_1 = -0.94J_3$, $J_2 = -0.16J_3$ and $J_6 = 0.15J_3$ in combination with a g value of 2.20. Given the strongly distorted octahedral Cu^{2+} environment, implying anisotropic g values ranging from $0.1 \leq \Delta g/g \leq 0.15$ [24, 25], a g value of 2.2 for $B \parallel c$ is reasonable. The values of the exchange couplings are within the error bars of the DFT calculation confirming that the DFT analysis of barlowite is reliable.

The inset of Fig. 5 exhibits the effective magnetic moment n_{eff} per Cu^{2+} ion as a function of temperature for $T \leq 100$ K in fields $B = 0.1$ T for $B \parallel c$ and $B \perp c$ both

after cooling in zero field (ZFC). At 300 K (not shown) n_{eff} is about $1.69 \mu_B/\text{Cu}^{2+}$, a value slightly smaller than the one for isolated spin-1/2 ions. With decreasing temperature n_{eff} becomes continuously reduced down to approximately $1.2 \mu_B$ around 20 K. Such a large effective moment in an antiferromagnetically coupled system at a temperature $T \lesssim J_3/10$ is only possible when in addition a ferromagnetic coupling exists which is of similar size. Upon cooling to below about 18 K, n_{eff} for both orientations starts to increase with a maximum slope around 15 K. Upon further cooling, n_{eff} passes over a maximum followed by a rapid decrease. This behavior is a clear signature of a phase transition into long-range antiferromagnetic order characterized by canted spins exhibiting a small ferromagnetic component. This is also corroborated by the observation of a hysteresis loop observed at 2 K and shown in Fig. 5. The maximum of n_{eff} for the field aligned parallel to the hexagonal planes exceeds that for fields oriented perpendicular to the planes by nearly a factor of two, indicating that the easy axis of barlowite is oriented along the hexagonal plane.

Figure 6 exhibits the magnetization measured for $B \parallel c$ at 2 K. The blue open squares correspond to the virgin curve taken after cooling in zero field. This was possible after carefully compensating for finite remanent fields present in the superconducting magnet of the SQUID magnetometer. Also shown is the full hysteresis loop obtained upon cycling the field in the range $-5 \text{ T} \leq B \leq +5 \text{ T}$. The hysteresis loop closes at $|B| \geq 4 \text{ T}$ at 2 K, cf. lower right inset to Fig. 6. Upon field cycling (red symbols), following the virgin run, the magnetization exhibits a large slope for fields below 0.1 T. At this field level, M reaches approximately 10% of the expected saturation magnetization of $1 \mu_B$ per Cu^{2+} ion. On further increasing the field $M(B)$ increases almost linearly and reaches a value of $0.23 \mu_B/\text{Cu}^{2+}$ at 5 T, which is close to $1 \mu_B/\text{f.u.}$ The evolution of M upon varying B indicates a discontinuous magnetization process which has to be taken into account when analyzing magnetic data taken at fields below 4 T. The upper inset of Fig. 6 shows the low-field sector of the hysteresis loop. For $B = 0$ barlowite has a remanent magnetization of approximately $0.3 \mu_B$ per formula unit. According to Ref. 26 this value together with the saturation magnetization can be used to determine the tilt angle relative to the perfectly antiferromagnetically aligned spins resulting in a canting angle of approximately 4.5° . Such a moderate spin canting out of the hexagonal plane is consistent with the existence of a Dzyaloshinskii-Moriya (DM) interaction allowed by symmetry in barlowite. According to Ref. [27], the DM vector \mathbf{D} lies within the mirror plane which in barlowite is perpendicular to the kagome plane. An estimate of the size of $|\mathbf{D}|$ is given by $|\mathbf{D}|/J_3 \simeq \Delta g/g = 0.1$ which is substantial.

In summary, the structure of barlowite with perfectly aligned kagome layers opens a new synthetic route for

kagome-based structures with the possibility of interesting phases such as ordered magnetic phases with different ordering vectors, spin liquid, Dirac metal or even unconventional superconductivity. Our combined first principles calculations with susceptibility measurements identifies the low temperature behavior of barlowite as a canted antiferromagnet with a canting angle of approximately 4.5° .

Acknowledgements.— We would like to thank the Deutsche Forschungsgemeinschaft for financial support through the collaborative research unit TRR/SFB 49. F.S.-P. gratefully acknowledges the support of the Alexander von Humboldt Foundation through a Humboldt Research Fellowship. J.A.S. acknowledges support from the Independent Research/Development program while serving at the National Science Foundation.

-
- [1] M. P. Shores, E. A. Nytko, B. M. Bartlett and D. G. Nocera, *J. Am. Chem. Soc.* **127**, 13462 (2005).
 - [2] P. Mendels and F. Bert, *J. Phys. Soc. Jpn.* **79**, 011001 (2010).
 - [3] P. Mendels and F. Bert, *J. Phys.: Conf. Series* **320**, 012004 (2011).
 - [4] S.-H. Lee, H. Kikuchi, Y. Qiu, B. Lake, Q. Huang, K. Habicht, and K. Kiefer, *Nat. Mater.* **6**, 853 (2007).
 - [5] R. H. Colman, A. Sinclair, and A. S. Wills, *Chem. Mater.* **23**, 1811 (2011).
 - [6] Y. Li, B. Pan, S. Li, W. Tong, L. Ling, Z. Yang, J. Wang, Z. Cheng, Z. Wu and Q. Zhang, *New J. Phys.* **16**, 093011 (2014).
 - [7] Y.-S. Li, Q.-M. Zhang, *J. Phys. Condens. Matter* **25**, 026003 (2013).
 - [8] P. A. Lee, *Science* **321**, 1306 (2008).
 - [9] Y. Shimizu, K. Miyagawa, K. Kanoda, M. Maesato, G. Saito, *Phys. Rev. Lett.* **91**, 107001 (2003).
 - [10] T. Itou, A. Oyamada, S. Maegawa, M. Tamura, R. Kato, *Phys. Rev. B* **77**, 104413 (2008).
 - [11] T.-H. Han, J. S. Helton, S. Chu, D. G. Nocera, J. A. Rodriguez-Rivera, C. Broholm, Y. S. Lee, *Nature* **492**, 406 (2012).
 - [12] D. E. Freedman, T. H. Han, A. Prodi, Peter Müller, Q.-Z. Huang, Y.-S. Chen, S. M. Webb, Y. S. Lee, T. M. McQueen, and D. G. Nocera, *J. Am. Chem. Soc.* **132**, 16185 (2010).
 - [13] T. Hanisch, G. S. Uhrig, and E. Müller-Hartmann, *Phys. Rev. B* **56**, 13960 (1997).
 - [14] I. I. Mazin, H. O. Jeschke, F. Lechermann, H. Lee, M. Fink, R. Thomale, and R. Valentí, *Nat. Commun.* **5**, 4261 (2014).
 - [15] P. Elliott, and M. A. Cooper, *Mineralog. Mag.* **74**, 797 (2010).
 - [16] T.-H. Han, J. Singleton, and J. Schlueter, *Phys. Rev. Lett.* **113**, 227203 (2014).
 - [17] CCDC 1019246 contains the supplementary crystallographic data for this paper. These data can be obtained free of charge from The Cambridge Crystallographic Data Centre via www.ccdc.cam.ac.uk/data_request/cif.
 - [18] K. Koepnik and H. Eschrig, *Phys. Rev. B* **59**, 1743 (1999); <http://www.FPLO.de>
 - [19] J. P. Perdew, K. Burke, and M. Ernzerhof, *Phys. Rev. Lett.* **77**, 3865 (1996).
 - [20] A. I. Liechtenstein, V. I. Anisimov, and J. Zaanen, *Phys. Rev. B* **52**, R5467 (1995).
 - [21] K. Foyevtsova, I. Opahle, Y.-Z. Zhang, H. O. Jeschke, R. Valentí, *Phys. Rev. B* **83**, 125126 (2011).
 - [22] H. O. Jeschke, F. Salvat-Pujol, R. Valentí, *Phys. Rev. B* **88**, 075106 (2013).
 - [23] A. Lohmann, H.-J. Schmidt, J. Richter, *Phys. Rev. B* **89**, 014415 (2014).
 - [24] B. L. Silver and D. Getz, *J. Chem. Phys.* **61**, 638 (1973).
 - [25] V. E. Petrashen, Yu. V. Yablokov, and R. L. Davidovich, *Phys. Stat. Sol. B* **101**, 117 (1980).
 - [26] O. Kahn, *Molecular Magnetism*, VCH, Weinheim-New York, 1993.
 - [27] T. Moriya, *Phys. Rev.* **120**, 91 (1960).